Carbohydrate Polymers 103 (2014) 456–465

Contents lists available at ScienceDirect

Carbohydrate Polymers

journal homepage: www.elsevier.com/locate/carbpol

# Preparation and characterization of bio-nanocomposite films of agar and silver nanoparticles: Laser ablation method

Jong-Whan Rhim[a,*], Long-Feng Wang[a], Yonghoon Lee[b], Seok-In Hong[c]

[a] Department of Food Engineering and Bionanocomposite Research Institute, Mokpo National University, 61 Dorimri, Chungkyemyon, Muangun, 534-729 Jeonnam, Republic of Korea
[b] Department of Chemistry, Mokpo National University, 61 Dorimri, Chungkyemyon, Muangun, 534-729 Jeonnam, Republic of Korea
[c] Korea Food Research Institute, 516 Baekhyun-dong, Bundang-gu, Seongnam-si, 463-746 Gyonggi-do, Republic of Korea

ARTICLE INFO

*Article history:*
Received 4 October 2013
Received in revised form
23 December 2013
Accepted 26 December 2013
Available online 5 January 2014

*Keywords:*
Laser ablation
Silver nanoparticles
Agar
Bio-nanocomposites
Antimicrobial activity

ABSTRACT

Silver nanoparticles (AgNPs) were prepared by a laser ablation method and composite films with the AgNPs and agar were prepared by solvent casting method. UV–vis absorbance test and transmission electron microscopy (TEM) analysis results revealed that non-agglomerated spherical AgNPs were formed by the laser ablation method. The surface color of the resulting agar/AgNPs films exhibited the characteristic plasmonic effect of the AgNPs with the maximum absorption peaks of 400–407 nm. X-ray diffraction (XRD) test results also exhibited characteristic AgNPs crystals with diffraction peaks observed at 2$\theta$ values of 38.39°, 44.49°, and 64.45°, which were corresponding to (1 1 1), (2 0 0), and (2 2 0) crystallographic planes of face-centered cubic (fcc) silver crystals, respectively. Thermogravimetric analysis (TGA) results showed that thermal stability of the agar/AgNPs composite films was increased by the inclusion of metallic silver. Water vapor barrier properties and surface hydrophobicity of the agar/AgNPs films increased slightly with the increase in AgNPs content but they were not statistically significant ($p > 0.05$), while mechanical strength and stiffness of the composite films decreased slightly ($p < 0.05$). The agar/AgNPs films exhibited distinctive antimicrobial activity against both Gram-positive (*Listeria monocytogenes*) and Gram-negative (*Escherichia coli* O157:H7) bacterial pathogens.



## 1. Introduction

Silver has long been recognized as an effective antimicrobial agent with a broad spectrum of antimicrobial activity against not only both Gram-positive and Gram-negative pathogenic bacteria but also viruses and other eukaryotic microorganisms (Russell & Hugo, 1994). Accordingly, with the advent of nanotechnology, silver nanoparticles (AgNPs) have been emerged in the development of an antibacterial, antifungal, antiviral, and anti-inflammatory agent (Rai, Yadav, & Gade, 2009; Vaidyanathan, Kalishwaralal, Gopalram, & Gurunathan, 2009). Especially, in food packaging sectors, AgNPs have been exploited for the preparation of antimicrobial active food packaging films due to their strong antimicrobial activity with high thermal stability (Llorens, Lloret, Picouet, Trbojevich, & Fernandez, 2012).

The antimicrobial efficiency of AgNPs-included antimicrobial packaging films is greatly influenced by various factors such as particle size, and its distribution, degree of particle agglomeration, silver content, and interaction of silver surface with the base polymer (Kim et al., 2007). Above all, AgNPs should be well dispersed through polymer matrix without agglomeration. Therefore, it is essential to obtain AgNPs with proper dimensions and to choose proper polymeric materials for the preparation of efficient antimicrobial packaging films with AgNPs.

Conventionally, AgNPs have been produced by the reduction of silver nitrate ($AgNO_3$) using chemical reducing agents such as sodium borohydride, dimethyl formamide, triethanolamine, and hydrazine (Yoksan & Chirachanchai, 2010). However, such chemical reduction method is not recommended since the chemicals are highly reactive and known to pose a potential environmental hazard and biological risks. Instead, a variety of green technologies for the preparation of AgNPs have been developed (Habbalalu, Lalley, Nadagouda, & Varma, 2013). For example, biological materials such as plant extracts, bacteria, fungi, and yeast have been used as mediators for the synthesis of AgNPs (Rhim, Wang, & Hong, 2013). Recently, another type of green technology has been tested using various carbohydrates such as glucose, sucrose, starch, chitosan, and marine polysaccharides. In these technologies, the biopolymers act as both reducing and stabilizing agents and also as polymer matrix for carrying AgNPs (Rhim et al., 2013; Venkatpurwar & Pokharkar, 2011). Furthermore, these approaches using biopolymers are safe, biocompatible, nontoxic

* Corresponding author. Tel.: +82 61 450 2423; fax: +82 61 454 1521.
*E-mail addresses:* jwrhim@mokpo.ac.kr, jwrhim@hanmail.net (J.-W. Rhim).

0144-8617/$ – see front matter © 2014 Elsevier Ltd. All rights reserved.
http://dx.doi.org/10.1016/j.carbpol.2013.12.075

and environmentally friendly (Sharma, Yngard, & Lin, 2009). Also, various physical methods such as UV, γ-ray, and microwave irradiation, thermal treatment, photochemical process, and sonochemical process have been used for the preparation of AgNPs without hazardous chemical concerns (Yoksan & Chirachanchai, 2010).

Although there are many routes available for the synthesis of nanoparticles, there is an increasing need to develop high-yield, low-cost, non-toxic and environmentally friendly procedures. One of the newest such approaches for preparing AgNPs is a laser ablation method (Christopher, Alee, & Rao, 2011; Herrera, Padilla, & Hernandez-Rivera, 2013). This is based on the ablation of a solid target, i.e., metallic silver, by a pulsed laser beam. The target is usually located in a liquid environment and the ablated AgNPs are collected in the form of colloidal solution. This is a fast, straightforward, and easy method for preparing AgNPs compared to other methods, as it does not need multistep chemical synthetic procedures, long reaction times, and high temperatures. However, most of the published works are mainly focused on the preparation and characterization of AgNPs using the laser ablation method (Hajiesmaeilbaigi, Mohammadalipour, Sabbaghzadeh, Hoseinkhani, & Fallah, 2006; Zamiri, Zakaria, Ahangar, Sadrolhosseini, & Mahdi, 2010, 2011a, 2011b). Though several research works have been published about the preparation of antimicrobial nanocomposite films by incorporation of AgNPs, produced by the reduction of $AgNO_3$, into the biopolymers such as agar and chitosan (Rhim et al., 2013; Tripathi, Mehrotra, & Dutta, 2011), to date, there is no report on the synthesis of bionanocomposite films blended with polymer and AgNPs produced by the laser ablation method.

Hence, the present study was performed to synthesize AgNPs by the laser ablation method and to test the feasibility of production of biopolymer, agar-based nanocomposite films with the AgNPs. The nanocomposite films were characterized by determining their optical, mechanical, barrier, thermal, and antimicrobial properties.

## 2. Materials and methods

### 2.1. Materials

A square silver plate (2 cm × 2 cm, 1 mm thick, 99.99% purity) was procured from Sigma–Aldrich (St. Louis, MO, USA). Food grade agar was procured from Fine Agar Agar Co., Ltd. (Damyang, Jeonnam, Korea) and glycerol was purchased from Daejung Chemicals & Metals Co., Ltd. (Siheung, Gyonggido, Korea). Polyvinyl pyrrolidone (PVP) was purchased from Sigma–Aldrich (St. Louis, MO, USA) and all other reagents were of analytical grade.

### 2.2. Preparation of AgNPs

A Q-switched Nd:YAG laser (Brilliant b, Quantel, Les Ulis, France) with pulse duration of 8 ns and 10 Hz repetition rate at the fundamental wavelength of 1064 nm was employed for ablation of silver. A silver plate was located in cubic glass cell containing 150 mL of 5% PVP solution. The PVP solution was used as a stabilizing agent for ablated AgNPs, in which the AgNPs are kept from agglomeration through the capping of AgNPs by the PVP (Tsuji et al., 2008; Wang, Qiao, Chen, Wang, & Ding, 2005; Wang, Liu, Ji, Ren, & Ji, 2012). The PVP is a water-soluble polymer made from monomer *N*-vinylpyrrolidone and the U.S. Food and Drug Administration (FDA) has approved this chemical for many uses in medicine, pharmacy, cosmetics and packaging industries, and it is generally considered safe (FDA).

First, the silver plate was washed using ultrasonic bath for 30 min and then immersed in the PVP solution. The solution was stirred magnetically during the ablation process to disperse the produced AgNPs. The laser output power was 200 mJ/pulse. The laser beam was focused on the silver target surface through a plano-convex lens ($f$ = 7 cm). The ablation was carried out with different duration times, i.e., 2, 4, and 8 h. The resulting ablated AgNPs were 20, 40, and 80 mg, respectively, which were confirmed by weight difference of the silver plate before and after the laser ablation.

### 2.3. Characterization of AgNPs

AgNPs solution with the concentration of 20 mg of AgNPs in 150 mL of 5% PVP solution was prepared using the same ablation method for the characterizing the optical properties. UV–vis absorption spectra of the AgNPs solutions were obtained by using a pectrophotometer (Model US/Lamda 3B, Perkin Elmer Co., Santa Clara, CA, USA) in the range of 300–700 nm.

Shape and size of the prepared AgNPs were characterized using Field Emission Transmission Electron Microscopy (FE-TEM, JEM-2100F, JEOL Ltd., Japan) at accelerating voltage of 200 kV. For the TEM experiments, two different concentrations of sample (2 and 16 mg AgNPs/100 mL PVP solution) were prepared by the laser ablation. A drop of each prepared solution was deposited onto nickel grids coated with thin carbon film and left for 1 day to dry completely at room temperature.

### 2.4. Preparation of agar/AgNPs composite films

Film solutions were prepared by dissolving 4 g of agar powder into the AgNPs solution (0, 20, 40, and 80 mg AgNPs/150 mL) with 1.2 g of glycerol while mixing vigorously for 30 min at 90 °C using a magnetic stirrer. The film solution was cast onto a leveled Teflon film (Cole-Parmer Instrument Co., Chicago, IL, USA) coated glass plate (24 cm × 30 cm), then dried for about 24 h at room temperature following the method of Rhim et al. (2013). In the same way, the control agar film was prepared without AgNPs. The resultant film was peeled off from the casting surface.

All film samples were preconditioned in a constant temperature and humidity chamber at 25 °C and with 50% relative humidity (RH) for at least 48 h to normalize the moisture content. The thickness of films was measured using a micrometer (Dial Thickness gauge 7301, Mitutoyo, Tokyo, Japan) with an accuracy of 0.01 mm.

### 2.5. Color and transparency

Surface color of the films was measured using a Chroma meter (Konica Minolta, CR-400, Tokyo, Japan) following the method of Rhim et al. (2013). The optical properties of the films were tested by measuring UV–vis absorption and transmission of the films. UV–vis absorption measurements were performed in the range of 300–700 nm using a UV–vis spectrophotometer (Model 8451A, Hewlett–Packard Co., Santa Clara, CA, USA). Transparency of the film samples was expressed as the percent transmittance measured at 660 nm.

### 2.6. X-ray diffraction (XRD) analysis

Structures of agar and AgNPs-incorporated agar films were evaluated with XRD measurements using a PANalytical Xpert pro MRD diffractometer (Amsterdam, Netherlands), operated at 40 kV and 30 mA, equipped with Cu Kα radiation at a wavelength of 0.15406 nm. The samples were scanned over the range of diffraction angle $2\theta$ = 10–80° with a scanning rate of 0.5°/min at room temperature.

### 2.7. Microstructure and element analysis

Microstructure of agar and agar/AgNPs films was tested using a FE-SEM (Field Emission Scanning Electron Microscope; S-4800,

Hitachi Co., Ltd., Matsuda, Japan) operated at accelerating voltage ($V_{acc}$) of 1 kV and current ($I_e$) of 10 μA. Contents of elements in the films were determined using an EDS (Energy Dispersive X-ray Microscope; EMAX, Horiba Co., Ltd., Wycombe, UK) operated at $V_{acc}$ of 15 kV.

### 2.8. FT-IR analysis

FT-IR spectra of agar and agar/AgNPs films were obtained using an attenuated total reflectance-Fourier transform infrared (ATR-FTIR) spectrophotometer (TENSOR 37 spectrophotometer with OPUS 6.0 software, Billerica, MA, USA) in the range of 4000–500 $cm^{-1}$.

### 2.9. Thermal stability

The thermal stability of the film samples was tested with thermogravimetric analysis (TGA; Hi-Res TGA 2950 Thermogravimetric Analyzer, TA Instruments, New Castle, DE, USA). About 5 mg of each sample was heated from room temperature to 600 °C at a heating rate of 10 °C/min under a nitrogen flow (50 $cm^3$/min) to obtain TGA data. Derivative form of TGA (DTGA) was obtained using differentials of TGA values following the method of Rhim et al. (2013).

### 2.10. Mechanical properties

The mechanical properties of the films were analyzed by measuring the tensile strength (TS), elongation at break (EB), and elastic modulus (E) according to the standard ASTM method D 882-88 using an Instron Universal Testing Machine (Model 5565, Instron Engineering Corporation, Canton, MA, USA) equipped with a 0.5 kN load cell. Rectangular strips (2.54 cm × 10 cm) were cut from individually prepared film using a precision double blade cutter (model LB.02/A, Metrotec, S.A., San Sebastian, Spain). Initial grip separation was set at 50 mm and cross-head speed at 50 mm/min. The TS (MPa) was determined by dividing the maximum load (N) by the initial cross-sectional area ($m^2$) of the film sample. The EB (%) was determined by dividing the extension at rupture of the film by the initial length of the film and multiplied by 100. The $E$ (GPa) was calculated from the slope of the initial linear region of the stress–strain curve at small strain.

### 2.11. Water vapor permeability (WVP) and water contact angle (CA)

The WVP of film sample was determined at 25 °C under 50% RH conditions using water vapor transmission measuring cups in accordance with the ASTM E96-95 standard method following the method of Rhim et al. (2013).

The contact angle of water in air on the film surface was measured using a CA analyzer (Model Phoenix 150, Surface Electro Optics Co., Ltd., Kunpo, Korea) after a water drop of ca. 10 μL was placed on the surface of film using a micro syringe.

### 2.12. Antibacterial activity

The antibacterial activity of the films was analyzed against two foodborne pathogens, Gram-positive bacterium (*Listeria monocytogenes* ATCC-19111) and Gram-negative bacterium (*Escherichia coli* O157:H7 ATCC-11775) obtained from ATCC (The American Type Culture Collection, Manasa, VA, USA), using a viable cell count method (Rhim et al., 2013).

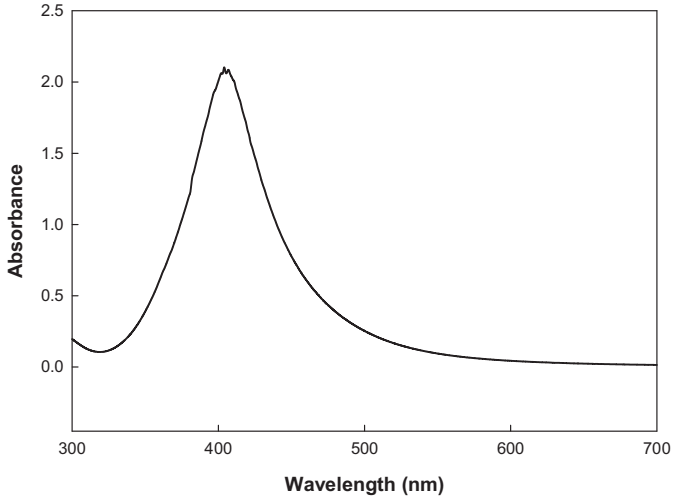


**Fig. 1.** UV–vis absorption spectra of AgNPs in PVP solution (13.3 mg AgNPs per 100 mL 5% PVP solution).

### 2.13. Statistical analysis

Film properties were measured with individually prepared films in triplicate. One-way analysis of variance (ANOVA) was performed, and the significance of each mean property value was determined ($p < 0.05$) with the Duncan's multiple range test of the statistical analysis system using the SPSS computer program (SPSS Inc., Chicago, IL, USA).

## 3. Results and discussion

### 3.1. Characterization of AgNPs

AgNPs were prepared by the direct laser ablation of silver plate in 5% PVP solution. Initially the PVP solution was colorless and transparent and it changed to yellowish brown and finally to brown as the laser ablation of silver plate progressed. Brown color development indicates the formation of AgNPs in the solution. The brown color intensity of solution increased with increase in ablation time, namely, with increase in AgNPs concentration. Brown coloration is the characteristic phenomenon of AgNPs, which has been frequently observed during the preparation of AgNPs not only in reduction of $AgNO_3$ by chemical or physical means (Temgire & Joshi, 2004) but also in the application of laser ablation methods (Zamiri et al., 2011a). The AgNPs are known to absorb radiation in the visible region of the electromagnetic spectrum (380–450 nm) due to the excitation of surface plasmon vibrations, and this is responsible for the characteristic yellow-brown color of AgNPs in various medium (Pandey, Goswami, & Nanda, 2012). Brown coloration of the 5% PVP solutions containing 20 mg AgNPs/150 mL was also confirmed by the UV–vis absorption spectra as shown in Fig. 1. A strong absorption peak was found in each spectrum around 407 nm. Zamiri et al. (2010, 2011a) also found similar absorption peaks at 403–413 nm and at 401–414 nm for AgNPs prepared by laser ablation of silver for different times in palm oil and coconut oil, respectively. It has been postulated that AgNPs are formed via nucleation, transition, and crystal growth of materials that were emitted from the silver plate upon laser ablation (Yang, 2007). There were no peaks observed at 335 and 560 nm (Fig. 1), which indicates no nanoparticles aggregation or nanocluster formed in the solution. As a result, the AgNPs formed by this method is highly stable and well dispersed in the solution (Pandey et al., 2012). In addition, the plasmon bands observed in the absorption spectra are symmetric in shape,

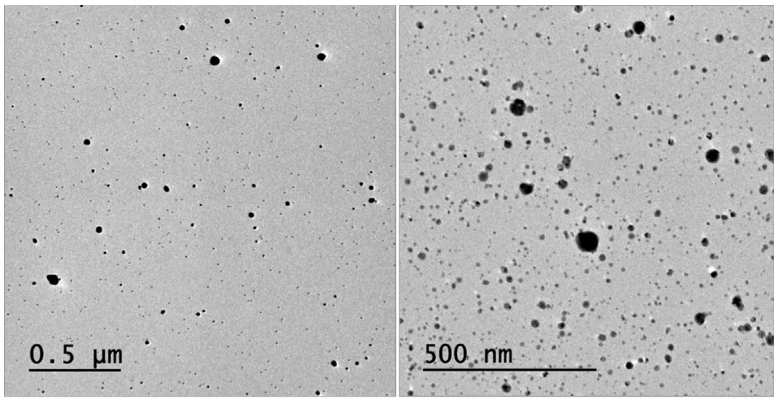


**Fig. 2.** TEM images of AgNPs in PVP solution.

**Table 1**
Apparent color values and transmittance ($T_{660\,nm}$) of agar and agar/AgNPs composite films.

| Film | $L$ | $a$ | $b$ | $\Delta E$ | $T_{660\,nm}$ (%) |
|---|---|---|---|---|---|
| Agar control | 92.23 ± 0.18$^{d}$ | −0.67 ± 0.04$^{a}$ | 6.29 ± 0.21$^{a}$ | 3.99 ± 0.28$^{a}$ | 87.5 ± 0.4$^{d}$ |
| Agar/AgNPs 20 mg | 51.75 ± 5.00$^{c}$ | 9.61 ± 1.23$^{c}$ | 27.53 ± 3.72$^{c}$ | 50.55 ± 2.8$^{b}$ | 56.4 ± 5.3$^{c}$ |
| Agar/AgNPs 40 mg | 32.80 ± 2.80$^{b}$ | 8.05 ± 2.60$^{c}$ | 11.34 ± 3.05$^{b}$ | 62.98 ± 1.91$^{c}$ | 29.2 ± 6.7$^{b}$ |
| Agar/AgNPs 80 mg | 28.19 ± 1.01$^{a}$ | 1.66 ± 0.67$^{b}$ | 6.82 ± 0.55$^{a}$ | 66.47 ± 0.96$^{d}$ | 11.0 ± 1.6$^{a}$ |

Each value is the mean of three replicates with the standard deviation. Any two means in the same column followed by the same letter are not significantly ($p > 0.05$) different by Duncan's multiple range tests.

which also indicates that the solution does not contain many aggregated particles (Pandey et al., 2012).

Fig. 2 shows TEM images of different concentration of AgNPs prepared by the laser ablation method. TEM images exhibits that the AgNPs are spherical in shape and they are well-scattered without agglomeration in the solution. Approximate sizes of AgNPs determined using internal scale of TEM were 20–25 and 48–51 nm for 1 mg and 8 mg AgNPs, respectively. Generally, the particle size of AgNPs prepared by the laser ablation looks bigger than those prepared by chemical reduction of $AgNO_3$ (Rhim et al., 2013). The AgNPs formed by the laser ablation of silver plate in the PVP solution were combined with PVP to form a microemulsion. The microemulsion system can protect the AgNPs from aggregation and act as a stabilizer for the AgNPs (Wang et al., 2005; Tsuji et al., 2008). Formation of well-scattered AgNPs with non-agglomerated spheres has been also observed in the laser ablation of silver in other solutions (Zamiri et al., 2010, 2011a).

### 3.2. Apparent film color

Apparent color and transparency of the agar and agar/AgNPs composite films are shown in Table 1. The control agar/PVP film was colorless and transparent, but agar/AgNPs composite films were yellowish-brown, brown, and dark brown depending on the concentration of AgNPs. The effect of inclusion of AgNPs and their concentration on the color change is clearly shown in the surface color values of the films. The lightness (Hunter $L$-values) of the composite films decreased significantly ($p < 0.05$) compared with the control film and the degree of decrease was dependent on the concentration of AgNPs. Hunter $a$- and $b$-values of agar films were also increased significantly after formation of nanocomposite with AgNPs due to their brown coloration. However, both Hunter $a$- and $b$-values of agar/AgNPs composite films decreased with increase in the silver particle concentration. Total color difference ($\Delta E$) values were also increased depending on the concentration of AgNPs. On the contrary, the transparency of the films decreased significantly depending on the concentration of AgNPs. The agar/AgNPs composite film with the smallest amount of AgNPs (20 mg) was still transparent, but the composite films with 40 mg and 80 mg of AgNPs were translucent and opaque, respectively. Similar behaviors of color and transmittance have been observed in agar/AgNPs films prepared through reduction of $AgNO_3$ (Rhim et al., 2013).

### 3.3. Optical properties

Absorption spectra of agar and agar/AgNPs films are shown in Fig. 3. The control agar film did not show any absorption peak in the test range of wavelength, but the agar/AgNPs composite films exhibited absorption peaks around 420 nm. The absorption peak height increased as the concentration of AgNPs increased up to inclusion of 40 mg of AgNPs. The absorption maximum of agar/AgNPs film with higher content of AgNPs (80 mg) was not recorded since it is beyond the detection limit of the equipment. However, it is not unreasonable to say that its absorption peak is around 420 nm after interpolation of the absorption spectrum. The absorption peak of the agar/AgNPs films is due to the plasmon resonance effect of the AgNPs formed by laser ablation of silver plate (Zamiri et al., 2010, 2011a, 2012). The optical plasmon resonance absorption peak of agar/AgNPs composite films was shifted to longer wavelength compared with that of AgNPs solutions shown in Fig. 1. It is probably due to the increased particle size caused by the agglomeration of the nanoparticles in much higher content of AgNPs for the preparation of the composite films. According to the Mie theory, the shift of maximum absorption peak to longer wavelength is related to the increase in particle size (Wriedt, 2012; Zamiri et al., 2012), and it is also known that aggregation of nanoparticles shifts the surface plasmon resonance (SPR) toward longer wavelengths (Ganeev, Baba, Ryasnyanskiĭ, Suzuki, & Kuroda, 2005).

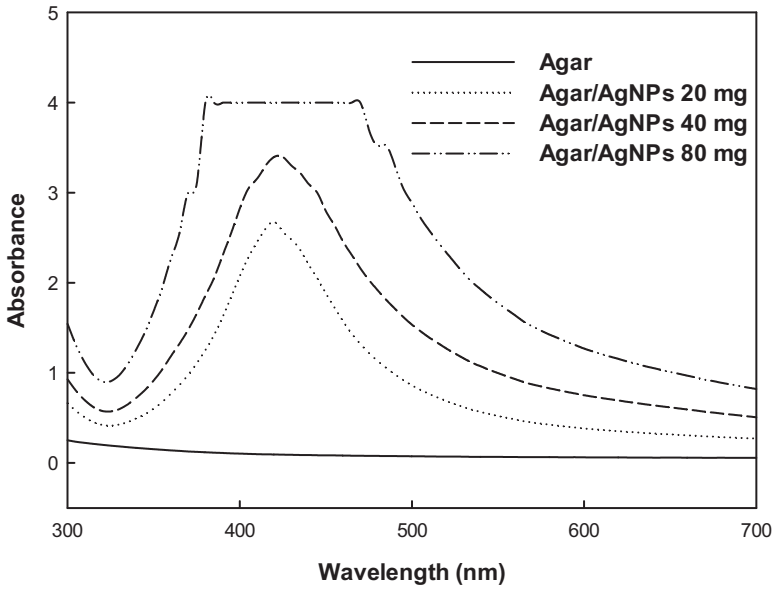


**Fig. 3.** UV–vis absorption spectra of agar and agar/AgNPs composite films.

### 3.4. Microstructure and element analysis

The microstructure of surface of agar and agar/AgNPs films was observed and analyzed by the FE-SEM coupled with an EDS detector, and the results are shown in Fig. 4. The SEM image showed the high density AgNPs and further confirmed that the agar/AgNPs films exhibit smooth surfaces with evenly dispersed silver particles. Clearly, the size of the AgNPs in the polymer matrix increased as the content of AgNPs increased and formed aggregation in the agar/AgNPs film with the highest content of AgNPs. These results are consistent with the results of optical property test. The SEM images also shows that the AgNPs formed are mostly spherical in shape.

Elements in the agar and agar/AgNPs films were determined by the EDS analysis and the results are presented in Table 2. The optical absorption band of the EDS peaks were observed in the range of 3–4 keV (data not shown), which is typical for the absorption of metallic silver nanocrystallites (Magudapaty, Gangopadhyay, Panigrahi, Nair, & Dhara, 2001). All of the agar/AgNPs films included the metallic element, Ag, and the amount of elemental silver in the agar/AgNPs composite films increased with the increase in the content of AgNPs. Similar SEM results were observed in agar/AgNPs films prepared by reduction of $AgNO_3$ (Rhim et al., 2013). In the process of agar/AgNPs film formation, the PVP molecules surrounding AgNPs can separate the nanoparticles one by one and become the joining between AgNPs and agar in the process of agar/AgNPs composite film formation. Therefore, the AgNPs disperse well in the nanocomposite film with uniform distribution of AgNPs in the polymer matrix (Tsuji et al., 2008; Wang, An, Luo, Li, & Li, 2008). However, more

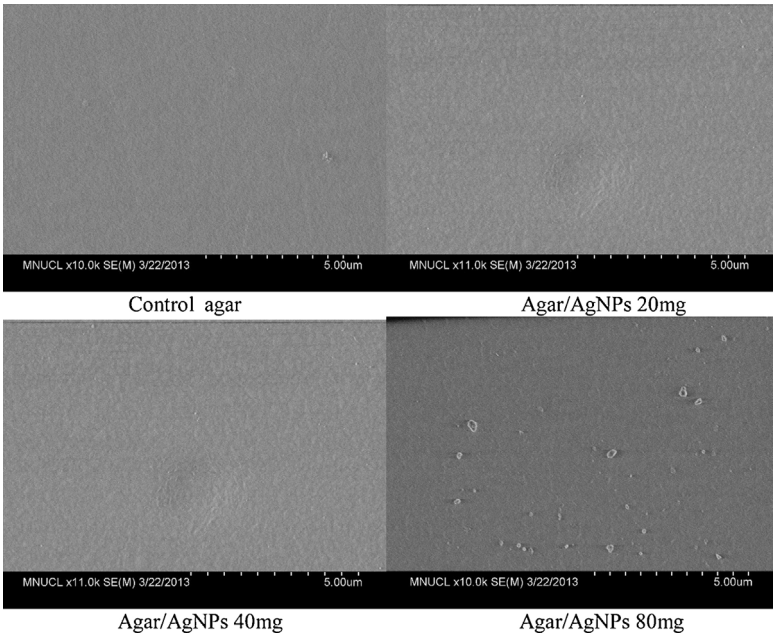


**Fig. 4.** SEM images of agar and agar/AgNPs composite films.

**Table 2**
Element analysis results of agar and agar/AgNPs composite films determined by EDS.

| Element | Agar film | Agar/AgNPs 20 mg | Agar/AgNPs 40 mg | Agar/AgNPs 80 mg |
|---|---|---|---|---|
| C | 46.47 | 62.99 | 64.64 | 62.28 |
| O | 52.74 | 34.36 | 31.27 | 32.25 |
| Na | 0.20 | 0.60 | 0.47 | 0.45 |
| S | 0.42 | 0.87 | 1.37 | 1.28 |
| Ca | 0.16 | 0.35 | 0.71 | 1.77 |
| Ag | – | 0.83 | 1.24 | 1.98 |

Expressed as percentage based on weight (wt%).

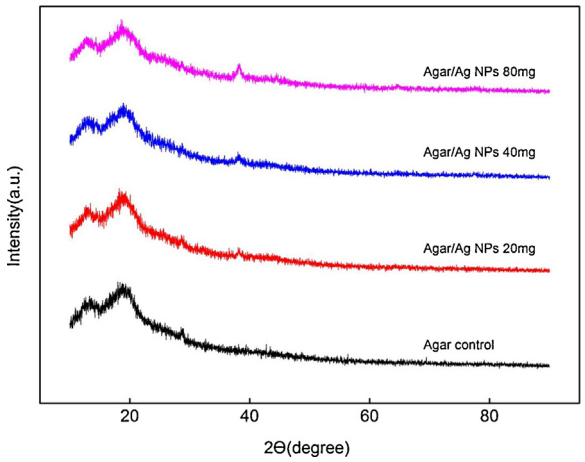


**Fig. 5.** XRD patterns of agar and agar/AgNPs composite films.

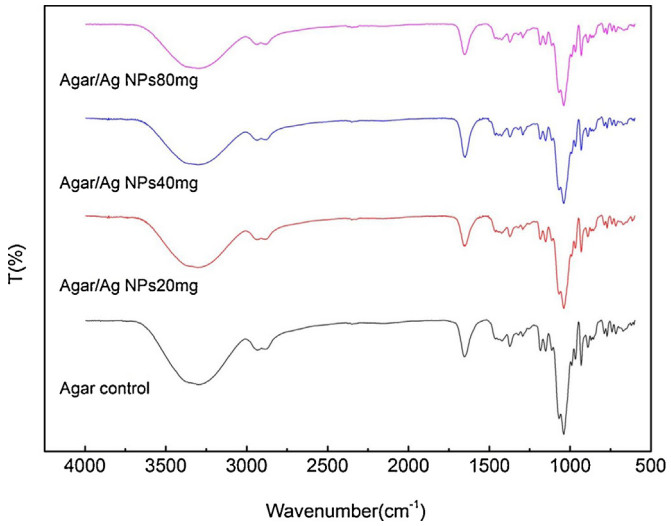


**Fig. 6.** FT-IR spectra of agar and agar/AgNPs composite films.

agglomerated AgNPs were observed in agar/AgNPs films prepared by laser ablation method compared with those prepared by the chemical reduction method at high concentration of nanoparticles.

### 3.5. XRD patterns

The crystalline nature of AgNPs in the films was tested by the X-ray diffraction (XRD) analysis. The XRD measurement results of the agar and agar/AgNPs films are shown in Fig. 5. The XRD patterns of agar/AgNPs composite films exhibit distinctive diffraction peaks at several positions of 2$\theta$ values. Basically two high intensity peaks with rather broad band were observed commonly at 2$\theta$ values of 10.23° and 18.01°, and a small peak at 28.57°. The diffuse broad peaks at 10.23° and 18.01° were attributed to the semi-crystalline agar polymer matrix (Rhim et al., 2013) and the third peak at 28.57° is probably attributed to PVP polymer added for the stabilization of AgNPs. In addition, several small diffraction peaks were observed at 2$\theta$ values of 38.39°, 44.49°, and 64.45° in the agar/AgNPs composite films, which were attributed to the formation of crystalline AgNPs. With increase in the AgNPs concentration, the number of diffraction and the peak height at specific diffraction position increased. These diffraction peaks, at 2$\theta$ = 38.39°, 44.49°, and 64.45°, are corresponding to (1 1 1), (2 0 0), and (2 2 0) crystallographic planes of face-centered cubic (fcc) silver crystals, respectively (Martínez-Castañón, Niño-Martinez, Martínez-Gutierrez, Martínez-Mendoza, & Ruiz, 2008; Rhim et al., 2013). The XRD results also indicate that the formation of silver crystal types was influenced by the concentration of AgNPs. As shown in Fig. 5, (1 1 1), (2 0 0), and (2 2 0) crystallographic planes of fcc silver crystal have been developed in the composite films prepared with high concentration of AgNPs (80 mg), while only (1 1 1) crystallographic plane of fcc silver crystal has been developed in the composite films with low concentration of AgNPs (20 mg and 40 mg). There was no clear peaks for (2 0 0) and (2 2 0) crystallographic planes of fcc silver crystals observed in the spectrum with low concentration of AgNPs, because their concentration was too low to be detected by XRD.

### 3.6. FT-IR analysis

Fig. 6 shows the FT-IR spectra of agar and agar/AgNPs composite films. The agar and agar/AgNPs nanocomposites films showed the absorption band at about 3308 and 2914 $cm^{-1}$, which are attributed to O—H stretching and methoxyl groups (C—H stretching vibration), respectively (Tako, Higa, Medoruma, & Nakasone, 1999). The band at around 1656 $cm^{-1}$ is due to the stretching vibration of the conjugated peptide bond formed by amine (NH) and acetone (CO) groups (Cristiaen & Bodard, 1983). This band intensity increased slightly in the composite films due to the presence of AgNPs. The peak at 1370 $cm^{-1}$ is attributed to ester sulfate, and the bands at 1070 and 931 $cm^{-1}$ are associated with the 3,6-anhydro-galactose bridges (Chirapart, Ohno, Ukeda, Sawamura, & Kusunose, 1995). The peak at 890 $cm^{-1}$ is attributed to the C—H of residual carbons of β-galactose (Matsuhiro, 1996). As a whole, all the FT-IR spectra of agar/AgNPs composite films are similar to that of agar film without formation of additional peaks, which suggests that no chemical bonds are formed between agar and AgNPs.

### 3.7. Thermal stability

The thermal stability of the agar and agar/AgNPs composite films was measured using TGA, and the resulting TGA and DTGA curves are shown in Fig. 7. The TGA thermograms show the weight decreasing pattern of thermal decomposition of the films and the DTGA curves clearly exhibit the maximum decomposition temperature ($T_{max}$) (Rhim et al., 2013). The TGA thermograms show that the thermal decomposition of the agar and agar/AgNPs composite films followed multistep thermal decomposition. The initial

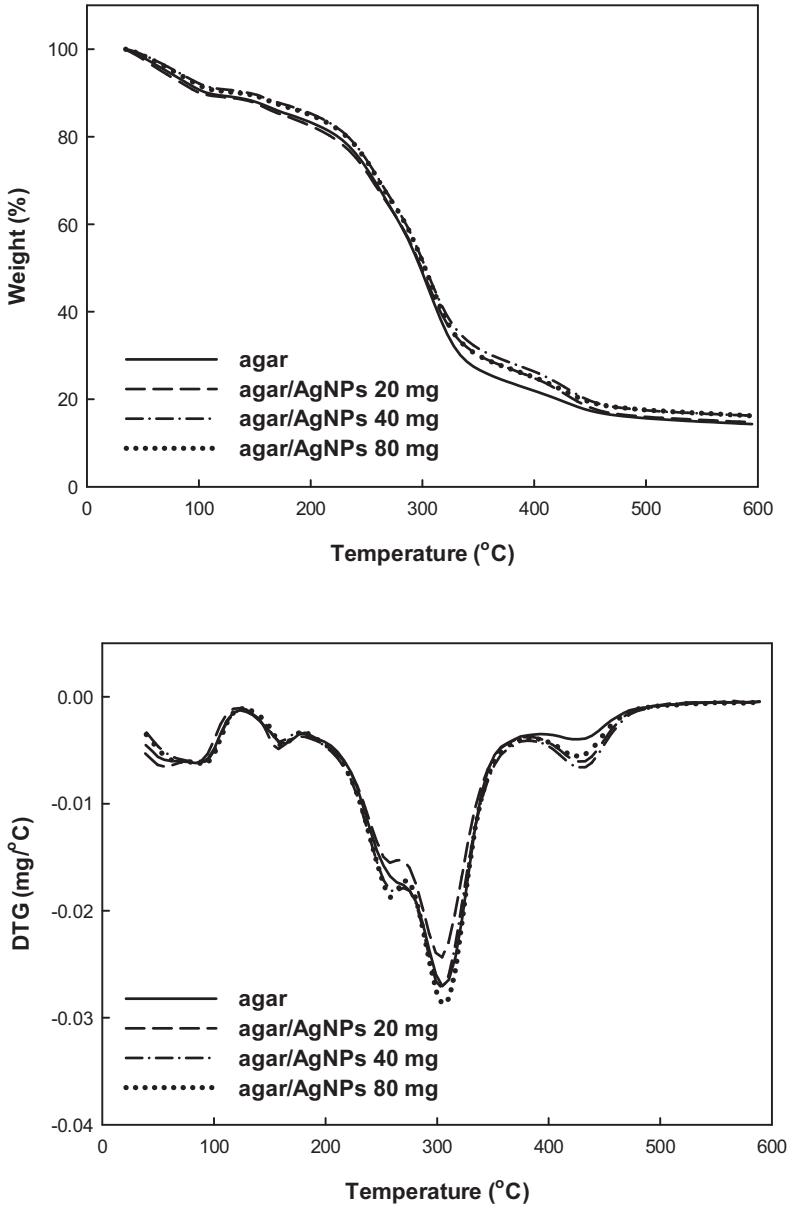


**Fig. 7.** TGA and DTGA curves of agar and agar/AgNPs composite films.

thermal decomposition was observed around 100 °C, which was due to the evaporation of moisture. In addition, small shoulders around 260 °C were observed due to the thermal decomposition of glycerol (Rhim et al., 2013). At the higher temperature around 300 °C, a major thermal decomposition was observed and can be attributed to the thermal decomposition of polymer agar (El-Hefian, Nasef, & Yahaya, 2012). The last thermal decomposition was observed around 440 °C, which was due to the thermal decomposition of PVP (Du, Yang, Mou, Hua, & Jiang, 2006). After the final thermal destruction, the residual percentages at 600 °C of the agar and agar/AgNPs films (with AgNPs content of 20, 40, and 80 mg) were 14.32%, 14.74%, 16.23%, and 16.24%, respectively. The high residuals of the agar/AgNPs composite films are mainly due to the inclusion of metallic AgNPs. In addition, the thermal destruction of AgNPs-loaded agar films delayed slightly compared with the neat agar film, indicating the increase in thermal stability, which is mainly due to the more heat stable metallic silver (Rhim et al., 2013).

### 3.8. Mechanical properties

Results of the tensile strength (TS) and elongation at break (EB), and elastic modulus (E) for the agar and agar/AgNPs films are shown in Table 3. The film thickness increased slightly with increase in the solid content. The TS of the control film was 49.58 ± 2.74 MPa, and it decreased up to 9% after formation of composite film with AgNPs. The decrease in the mechanical strength of the agar/AgNPs composite films is mainly because of no strong chemical bonds formation between AgNPs and the polymer matrices as evidenced by the FT-IR results. The mechanical force formed between agar and AgNPs is mainly caused by the less strong physical force between them such as coordination of the polymer with AgNPs through the hydroxyl functional groups of the polymeric chains and networks or physical adsorption of AgNPs (Pandey et al., 2012). Change in stiffness of the films determined by the elastic modulus ($E$) showed a similar trend as the TS, i.e., the stiffness of the composite films also decreased after blending with AgNPs except the low content

**Table 3**
Tensile properties of agar and agar/AgNPs composite films.

| Film | Thickness (μm) | TS (MPa) | EB (%) | *E* (GPa) |
|---|---|---|---|---|
| Agar control | 62.6 ± 1.2[a] | 49.58 ± 2.74[c] | 23.6 ± 4.0[b] | 1.43 ± 0.06[b] |
| Agar/AgNPs 20 mg | 62.2 ± 2.3[a] | 47.64 ± 2.20[bc] | 19.0 ± 3.1[a] | 1.46 ± 0.06[b] |
| Agar/AgNPs 40 mg | 64.5 ± 2.2[b] | 45.44 ± 1.99[ab] | 20.0 ± 4.3[b] | 1.34 ± 0.13[a] |
| Agar/AgNPs 80 mg | 65.8 ± 3.3[b] | 45.21 ± 5.51[a] | 21.3 ± 5.0[ab] | 1.29 ± 0.14[a] |

Each value is the mean of three replicates with the standard deviation. Any two means in the same column followed by the same letter are not significantly ($p > 0.05$) different by Duncan's multiple range tests.

**Table 4**
Water vapor permeability (WVP) and water contact angle (CA) of agar and agar/AgNPs composite films.

| Film | MC (%) | WVP ($\times 10^{-9}$ g m/m$^2$ Pa s) | CA (°) |
|---|---|---|---|
| Agar control | 16.6 ± 0.3[b] | 1.52 ± 0.06[a] | 47.31 ± 1.62[a] |
| Agar/AgNPs 20 mg | 16.1 ± 0.1[ab] | 1.51 ± 0.09[a] | 49.37 ± 1.27[b] |
| Agar/AgNPs 40 mg | 15.6 ± 0.2[a] | 1.41 ± 0.07[a] | 50.05 ± 0.83[b] |
| Agar/AgNPs 80 mg | 15.4 ± 0.7[a] | 1.38 ± 0.11[a] | 51.64 ± 0.38[c] |

Each value is the mean of three replicates with the standard deviation. Any two means in the same column followed by the same letter are not significantly ($p > 0.05$) different by Duncan's multiple range tests.

of AgNPs (20 mg). However, the flexibility of the composite films determined by the elongation at break (EB) was not significantly changed after formation of composite with AgNPs. Though the TS of agar/AgNPs films decreased slightly after formation of the composite films, they are still stronger than or comparable to those of commodity plastic films such as HDPE, LDPE, PP, PS, and PLA films (Rhim et al., 2013).

### 3.9. Water vapor permeability (WVP) and water contact angle (CA)

Results of the WVP of the agar and agar/AgNPs composite films are shown in Table 4. The WVP value of the control film was $(1.52 \pm 0.06) \times 10^{-9}$ g m/m$^2$ s Pa which is a little lower than that of agar films ($1.97 \times 10^{-9}$ g m/m$^2$ s Pa) previously reported by Rhim et al. (2013). The difference is mainly attributed to the PVP included for the preparation of agar films in the present study. Though there were no significant differences ($p > 0.05$) the WVP between the control and agar/AgNPs composite films, the addition of silver nanoparticles into the agar films resulted in a substantial decrease in the WVP, and the WVP decreased depending on the concentration of AgNPs. Similar result was observed with agar/AgNPs composite films prepared by reduction of $AgNO_3$ (Rhim et al., 2013). The decrease in WVP of the agar/AgNPs composite films may be presumably due to the increased tortuous pathway of the water vapor diffusion caused by the impervious AgNPs in the polymer matrix (Rhim et al., 2013). In addition, the AgNPs exist as a discontinuous phase in the film matrix preventing the mobility of polymer chains. The reduced mobility of polymer chains may induce the decrease in the WVP of the composite films (Su, Huang, Zhao, Yuan, & Li, 2010).

Surface hydrophobicity of the agar and agar/AgNPs composite films was determined by measuring the CA of water droplet on the surface of the films, and the results are also shown in Table 4. The CA of the control agar film was 47.31 ± 3.40°, which is consistent with previously reported values for agar films (Rhim, 2012; Rhim et al., 2013). The CA of the agar/AgNPs films increased significantly after formation of composite with AgNPs. The increase in the CA of the agar/AgNPs composite films was attributed to inclusion of hydrophobic metallic silver in the polymer matrix resulting in the increased surface hydrophobicity of the agar/AgNPs films (Rhim et al., 2013).

### 3.10. Antimicrobial activity

The antimicrobial activity of the agar and agar/AgNPs films was tested against Gram-positive (*L. monocytogenes*) and Gram-negative (*E. coli* O157:H7) foodborne pathogenic bacteria using a total viable cell count method, and the results are shown in Fig. 8. As expected, the control film did not show any antimicrobial activity against both Gram-positive and Gram-negative bacteria. However, the AgNPs containing composite films exhibited clear antimicrobial activity and their antimicrobial activity was dependent on the concentration of AgNPs and the type of microorganisms tested. Regardless of concentration of AgNPs, all the agar/AgNPs composite films exhibited only bacteriostatic activity against Gram-positive bacteria. However, the agar/AgNPs composite films showed distinctive antimicrobial activity against Gram-negative bacteria depending on the concentration of AgNPs. It showed slight antimicrobial activity with a low concentration of AgNPs (20 mg), but it exhibited potent antimicrobial activity with higher concentration of AgNPs (40 and 80 mg). This result agrees well with previously reported result of Rhim et al. (2013). The present result is also consistent with the well known belief that the AgNPs have stronger antimicrobial activity against Gram-negative bacteria than Gram-positive bacteria. The difference in antimicrobial activity of AgNPs between Gram-positive and Gram-negative bacteria can be explained partly by the difference in their cell structure. Gram-positive bacteria are composed of a three-dimensional thick peptidoglycan (20–80 nm) layer consisting of linear polysaccharide chains cross linked by more short peptides forming a complex structure, which makes it difficult for AgNPs to penetrate into Gram-positive bacteria (Priyadarshini, Gopinath, Meera Priyadharsshini, MubarakAli, & Velusamy, 2013). On the contrary, Gram-negative bacteria are coated with negatively charged outer membrane of thin peptidoglycan layer (7–8 nm) which can facilitate AgNPs to penetrate into Gram-negative bacteria (Priyadarshini et al., 2013).

Although a clear mechanism for the antimicrobial activity of AgNPs has not been established yet, several mechanistically probable functions of AgNPs have been reported. One of the most widely accepted one is that positively charged silver ions can interact with negatively charged phosphorus or sulfur containing biomacromolecular compounds (proteins and nucleic acids), causing structural changes and deformation in bacterial cell walls and membranes that leads to disruption of metabolic processes followed by cell death (Butkus, Edling, & Labare, 2003). It is also believed that the antimicrobial action of silver nanoparticles depends on the surface area of nanoparticles which are most likely to act as reservoirs for releasing the Ag ions (Feng et al., 2000). The antimicrobial mechanism of silver nanoparticles has also been suggested to be related with membrane damage due to free radicals derived from the surface of the nanoparticles causing a significant increase in membrane permeability and leading to cell death (Kim et al., 2007; Sondi & Salopek-Sondi, 2004).

The agar/AgNPs composite films, prepared by the laser ablation method, with strong antimicrobial activity are expected to have high potential as an antimicrobial food packaging material. However, there is also a concern on the safety of nanoparticles including

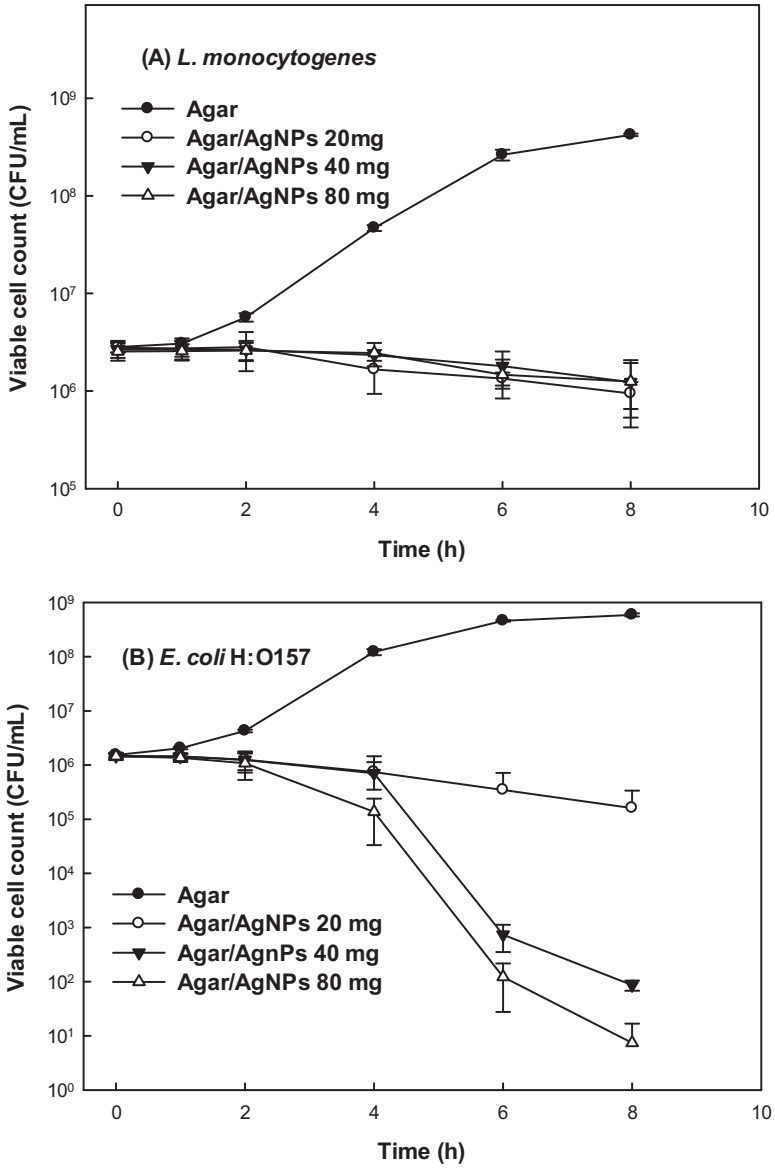


**Fig. 8.** Antimicrobial activity of agar and agar/AgNPs composite films against *L. monocytogenes* and *E. coli* O157:H7.

AgNPs, especially for their application as food contact packaging materials. Presently, very little information is available to assess the safety on human beings and the effect on the ecosystem of AgNPs migrated from the packaging materials (Duncan, 2011). Therefore, it is difficult to broadly assess the aspect of the safety of AgNPs-based food contact materials at this time.

## 4. Conclusion

AgNPs were obtained by a novel technology of the laser ablation of silver plate in a PVP solution used as a stabilizer for the AgNPs. The AgNPs prepared by the laser ablation method exhibited unique surface plasmonic effect of AgNPs as observed in the AgNPs prepared by reduction of $AgNO_3$. Free-standing composite films with agar and AgNPs obtained by the laser ablation method were prepared by a solution casting method. The resulting agar/AgNPs composite films had homogeneous distribution of AgNPs in the polymer matrix, and their properties were affected by the content of AgNPs included. The apparent color of the composite films varied from yellowish brown to dark brown depending on the concentration of AgNPs. The water vapor barrier properties and surface hydrophobicity of the agar film increased with slight decrease in the mechanical strength after formation of composite with AgNPs. In addition, the agar/AgNPs composite films exhibited distinctive antimicrobial activity against both the Gram-positive and Gram-negative pathogenic bacteria, though they showed stronger antimicrobial activity against Gram-negative bacteria than Gram-positive bacteria. In conclusion, the laser ablation method can be used as an effective green method for the preparation of AgNPs and the resulting agar/AgNPs composite films with definite antimicrobial activity are expected to be used as an active packaging application such as an antimicrobial food packaging or a biomedical application such as wound dressings.

## Acknowledgements

This research was supported by R&D Convergence Support Program (ARC 710003) of the Ministry for Agriculture, Food and Rural affairs, Republic of Korea. Assistance of Yongdeuk Gong and Heesigi Kim for the laser ablation works is acknowledged.

## References


Butkus, M. A., Edling, L., & Labare, M. P. (2003). The efficacy of silver as a bactericidal agent: Advantages, limitations and considerations for future use. *Journal of Water Supply: Research and Technology-AQUA*, *52*, 407–416.

Chirapart, A., Ohno, M., Ukeda, H., Sawamura, M., & Kusunose, H. (1995). Chemical composition of agars from a newly reported Japanese agarophyta, *Gracilariopsis lemaneiformis*. *Journal of Applied Phycology*, *7*, 359–365.

Christopher, D., Alee, K. S., & Rao, D. N. (2011). Synthesis and characterization of silver nanoparticles produced by laser ablation technique in aqueous monomer solution. *Journal of Trends & Chemistry*, *2*(1), 1–5.

Cristiaen, D., & Bodard, M. (1983). Spectroscopie infrarouge de films d'agar de *Gracilaria verrucosa* (Huds) papefuss. *Botanica Marina*, *26*, 425–427.

Du, Y. K., Yang, P., Mou, Z. G., Hua, N. P., & Jiang, L. (2006). Thermal decomposition behaviors of PVP coated on platinum nanoparticles. *Journal of Applied Polymer Science*, *99*, 23–26.

Duncan, T. V. (2011). Applications of nanotechnology in food packaging and food safety: Barrier materials, antimicrobials and sensors. *Journal of Colloid and Interface Science*, *363*, 1–24.

El-Hefian, E. A., Nasef, M. M., & Yahaya, A. H. (2012). Preparation and characterization of chitosan/agar blended films: Part 2. Thermal, mechanical, and surface properties. *E-Journal of Chemistry*, *9*, 510–516.

FDA. (2010). *Inactive ingredients in FDA approved drugs*. FDA/Center for Drug Evaluation and Research, Office of Generic Drugs, Division of Labeling and Program Support. http://www.accessdata.fda.gov/scripts/cder/iig/index.cfm (January 13, 2010)

Feng, Q. L., Wu, J., Chen, G. Q., Cui, F. G., Kim, T. N., & Kim, J. O. (2000). A mechanistic study of the antibacterial effect of silver ions on *Escherichia coli* and *Staphylococcus aureus*. *Journal of Biomedical Materials Research*, *52*, 662–668.

Ganeev, R. A., Baba, M., Ryasnyanskiĭ, A. I., Suzuki, M., & Kuroda, H. (2005). Laser ablation of silver in different liquids: Optical and nonlinear optical properties of silver nanoparticles. *Optics and Spectroscopy*, *99*, 668–676.

Habbalalu, D., Lalley, J., Nadagouda, M. N., & Varma, R. S. (2013). Green techniques for the synthesis of silver nanoparticles using plant extracts, enzymes, bacteria, biodegradable polymers, and microwaves. *Sustainable Chemistry & Engineering*, *1*, 703–712.

Hajiesmaeilbaigi, F., Mohammadalipour, A., Sabbaghzadeh, J., Hoseinkhani, S., & Fallah, H. R. (2006). Preparation of silver nanoparticles by laser ablation and fragmentation in pure water. *Laser Physics Letter*, *3*, 252–256.

Herrera, G. M., Padilla, A. C., & Hernandez-Rivera, S. P. (2013). Surface enhanced Raman scattering (SERS) studies of gold and silver nanoparticles prepared by laser ablation. *Nanomaterials*, *3*, 158–172.

Kim, J. S., Kuk, K. E., Yu, K. N., Kim, J. H., Park, S. J., Lee, H. J., et al. (2007). Antimicrobial effects of silver nanoparticles. *Nanomedicine: Nanotechnology, Biology, and Medicine*, *3*, 95–101.

Llorens, A., Lloret, E., Picouet, P. A., Trbojevich, R., & Fernandez, A. (2012). Metallic-based micro and nanocomposites in food contact materials and active food packaging. *Trends in Food Science & Technology*, *24*, 19–29.

Magudapaty, P., Gangopadhyay, P., Panigrahi, B. K., Nair, K. G. M., & Dhara, S. (2001). Electrical transport studies of Ag nanoclusters embedded in glass matrix. *Physica B: Condensed Matter*, *299*, 142–146.

Martínez-Castañón, G. A., Niño-Martinez, N., Martínez-Gutierrez, F., Martínez-Mendoza, J. R., & Ruiz, F. (2008). Synthesis and antibacterial activity of silver nanoparticles with different sizes. *Journal of Nanoparticle Research*, *10*, 1343–1348.

Matsuhiro, B. (1996). Vibrational spectroscopy of seaweeds galactans. *Hydrobiologia*, *326/327*, 481–489.

Pandey, S., Goswami, G. K., & Nanda, K. K. (2012). Green synthesis of biopolymer–silver nanoparticle nanocomposite: An optical sensor for ammonia detection. *International Journal of Biological Macromolecules*, *51*, 583–589.

Priyadarshini, S., Gopinath, V., Meera Priyadharsshini, N., MubarakAli, D., & Velusamy, P. (2013). Synthesis of anisotropic silver nanoparticles using novel strain. *Colloids and Surfaces B: Biointerfaces*, *102*, 232–237.

Rai, M., Yadav, A., & Gade, A. (2009). Silver nanoparticles as a new generation of antimicrobials. *Biotechnology Advances*, *27*, 76–83.

Rhim, J. W. (2012). Physical–mechanical properties of agar/κ-carrageenan blend film and derived clay nanocomposite film. *Journal of Food Science*, *77*(12), N66–N73.

Rhim, J. W., Wang, L. F., & Hong, S. I. (2013). Preparation and characterization of agar/silver nanoparticles composite films with antimicrobial activity. *Food Hydrocolloids*, *33*, 327–335.

Russell, A. D., & Hugo, W. B. (1994). Antimicrobial activity and action of silver. *Progress in Medicinal Chemistry*, *31*, 351–370.

Sharma, V. K., Yngard, R. A., & Lin, Y. (2009). Silver nanoparticles: Green synthesis and their antimicrobial activities. *Advances in Colloid and Interface Science*, *145*, 83–96.

Sondi, I., & Salopek-Sondi, B. (2004). Silver nanoparticles as antimicrobial agent: A case study of *E. coli* as a model for Gram-negative bacteria. *Journal of Colloid and Interface Science*, *275*, 177–182.

Su, J. F., Huang, Z., Zhao, Y. H., Yuan, X. Y., & Li, M. (2010). Structure and properties of carboxymethyl cellulose/soy protein isolate blend edible films cross linked by Maillard reactions. *Carbohydrate Polymers*, *79*, 145–153.

Tako, M., Higa, M., Medoruma, K., & Nakasone, Y. (1999). A highly methylated agar from red seaweed, *Gracilaria arcuata*. *Botanica Marina*, *42*, 513–518.

Temgire, M. K., & Joshi, S. S. (2004). Optical and structural studies of silver nanoparticles. *Radiation Physics and Chemistry*, *71*, 1039–1044.

Tripathi, S., Mehrotra, G. K., & Dutta, P. K. (2011). Chitosan–silver oxide nanocomposite film: Preparation and antimicrobial activity. *Bulletin of Material Science*, *34*, 29–35.

Tsuji, T., Thang, D. H., Okazaki, Y., Nakanishi, M., Tsuboi, Y., & Tsuji, M. (2008). Preparation of silver nanoparticles by laser ablation in polyvinylpyrrolidone solutions. *Applied Surface Science*, *254*, 5224–5230.

Vaidyanathan, R., Kalishwaralal, K., Gopalram, S., & Gurunathan, S. (2009). Nanosilver – The burgeoning therapeutic molecule and its green synthesis. *Biotechnology Advances*, *27*, 924–937.

Venkatpurwar, V., & Pokharkar, V. (2011). Green synthesis of silver nanoparticles using marine polysaccharide: Study of in-vitro antibacterial activity. *Materials Letters*, *65*, 999–1002.

Wang, D., An, J., Luo, Q., Li, X., & Li, M. (2008). A convenient approach to synthesize stable silver nanoparticles and silver/polystyrene nanocomposite particles. *Journal of Applied Polymer Science*, *110*, 3038–3046.

Wang, B. L., Liu, X. H., Ji, Y., Ren, K. F., & Ji, J. (2012). Fast and long-acting antibacterial properties of chitosan-Ag/polyvinylpyrrolidone nanocomposite films. *Carbohydrate Polymer*, *90*, 8–15.

Wang, H., Qiao, X., Chen, J., Wang, X., & Ding, S. (2005). Mechanisms of PVP in the preparation of silver nanoparticles. *Materials Chemistry and Physics*, *94*, 449–453.

Wriedt, T. (2012). Mie theory: A review. In W. Hergert, & T. Wriedt (Eds.), *The Mie theory: Basics and applications* (pp. 53–71). Berlin, Heidelberg: Springer-Verlag.

Yang, G. W. (2007). Laser ablation in liquids: Applications in the synthesis of nanocrystals. *Progress in Materials Science*, *52*, 648–698.

Yoksan, R., & Chirachanchai, S. (2010). Silver nanoparticle-loaded chitosan-starch based films: Fabrication and evaluation of tensile, barrier and antimicrobial properties. *Materials Science and Engineering: C*, *30*, 891–897.

Zamiri, R., Zakaria, A., Ahangar, H. A., Sadrolhosseini, A. R., & Mahdi, M. A. (2010). Fabrication of silver nanoparticles dispersed in palm oil using laser ablation. *International Journal of Molecular Science*, *11*, 4764–4770.

Zamiri, R., Zakaria, A., Ahangar, H. A., Sadrolhosseini, A. R., & Mahdi, M. A. (2011a). Preparation of silver nanoparticles in virgin coconut oil using laser ablation. *International Journal of Nanomedicine*, *6*, 71–75.

Zamiri, R., Zakaria, A., Ahangar, H. A., Sadrolhosseini, A. R., & Mahdi, M. A. (2011b). Laser-fabricated castor oil-capped silver nanoparticles. *International Journal of Nanomedicine*, *6*, 565–568.

Zamiri, R., Azmi, B. Z., Ahangar, H. A., Zamiri, Z., Husin, M. H., & Wahab, Z. A. (2012). Preparation and characterization of silver nanoparticles in natural polymers using laser ablation. *Bulletin of Materials Science*, *35*, 727–731.